Analysis of the haemodynamic changes caused by surgical and transcatheter aortic valve replacements by means fluid-structure interaction simulations

Anna Maria Tango [a,1] , Alessandra Monteleone [b,1] , Andrea Ducci [a], Gaetano Burriesci [a,b,c,*]

[a] *UCL Mechanical Engineering, University College London, UK*
[b] *Ri.MED Foundation, Palermo, Italy*
[c] *University of Palermo, Department of Engineering, Palermo, Italy*

ARTICLE INFO

ABSTRACT

Aortic valve replacements, both surgical and transcatheter, are nowadays widely employed treatments. Although clinically effective, these procedures are correlated with potentially severe clinical complications which can be associated with the non-physiological haemodynamics that they establish. In this work, the fluid dynamics changes produced by surgical and transcatheter aortic valve replacements are analysed and compared with an ideal healthy native valve configuration, employing advanced fluid-structure interaction (FSI) simulations. The aim of the study is to investigate how existing treatments may affect the aortic valve function, and giving indications about how to improve current therapies.

Simulations were performed using the commercial software LS-DYNA, where the FSI strategy is based on the coupling of a Lagrangian approach for the structures and a Eulerian approach for the fluid, whilst the coupling between the two domains is reached through a hybrid arbitrary-Lagrangian-Eulerian algorithm. Idealised geometries are used for the aortic root and leaflets. The aortic wall was modelled as linear elastic material, whilst leaflets were modelled as hyperelastic incompressible, using an Ogden's constitutive model. A combination of physiological flow velocity and pressure differences are applied as boundary conditions to model realistically the whole cardiac cycle.

Results are analysed throughout the cardiac cycle in terms of leaflets kinematics, flow dynamics, pressure and valve performance parameters. Globally, surgical valves presented worse performance than transcatheter counterparts (reduced effective orifice area, increased transvalvular pressure drop and increased opening and closing times). The clinical parameters of transcatheter devices were improved and closer to those of the healthy native valve, although the vortical activity within the Valsalva's sinuses was substantially altered. Here, the presence of the partition obstructed the washing out, resulting in higher degree of blood stasis and potential blood damage.

The implantation of prosthetic devices produces major haemodynamic changes which alters the valve dynamics and leads to diminished performance. Currently, the design of these substitutes is not optimised to mimic realistic native conditions, particularly in terms of valve opening behaviour. Although transcatheter devices provide systolic performance similar to that estimated for the healthy native aortic model, none of the prosthetic solutions appeared to be able to fully restore healthy physiological conditions.

1. Introduction

The aortic valve is a tri-leaflet heart valve that has the fundamental role of regulating the unidirectional flow of oxygenated blood from the heart to the body tissues, through the systemic circulation. This crucial and demanding function makes it particularly susceptible to relevant congenital or acquired diseases [1,2], which represent one of the leading causes of global cardiovascular morbidity and mortality [3,4].

Aortic valve replacement is intended to restore normal operating conditions by implanting a prosthetic device aimed at restoring the healthy physiological function minimising related complications [5]. A prosthetic device which does not introduces significant alterations in the normal haemodynamics, ensuring minimum transvalvular systolic pressure drops and avoiding disturbance to the healthy velocity field is highly desirable [6]. In this context, surgical and transcatheter aortic valve replacement procedures (respectively refereed as SAVR and TAVR) are common options for the aortic valve replacement. SAVR consists in removing the diseased aortic leaflets and replace the valve with a mechanical or biological artificial valve substitute, sutured to the native aortic annulus. Bioprosthetic valves present a more physiological haemodynamics than mechanical devices, attempting to mimic the native valve functioning through prosthetic leaflets made from biological soft-tissues [7]. However, they are still unable to replicate the behaviour of native valves, due to the presence of the supporting stent and the implantation procedure [8,9]. Stentless configurations, mitigating these limitations [10], may result into suboptimal and less repeatable operating configurations, due to more complex suturing and the irregularity of the host anatomy. In the last decades, TAVR has established as a far less invasive alternative to SAVR, especially suitable for patients unfit for surgery [11–13]. In this approach, the prosthetic leaflets are mounted on a stent which can be collapsed, delivered inside the native valve through the vasculature, and then re-expanded [14]. In this case, the aortic root anatomy plays an important role, as it represents the landing zone for the prosthesis and provides the mechanical response needed to securely anchor the valve. Similarly to stentless SAVR, transcatheter devices deployment can lead to an elliptical shape of the valve which, in turn, can result in coaptation mismatch [15]. Though the clinical benefit of the treatment has been clearly established, some post procedural complications have emerged. In particular, the occurrence of silent ischemic lesions and vascular dementia is considerably higher than with SAVR [16–18]. The source of these pathologies is still unclear, although a potential cause is identified in the haemodynamics perturbations produced downstream of the valve [19]. Moreover, with TAVR, the native valve is not removed from the anatomical site, but its leaflets are pushed towards the aortic root wall, becoming a physical barrier within the Valsalva sinuses region which can cause stagnation and blood damage [20].

A number of studies in the literature adopt *in vivo*, *in vitro* and *in silico* approaches to study the functioning of native and prosthetic valves, the correlation between mechanical stresses and valve diseases, and the interdependence between haemodynamics performance and post implantation complications [21,22]. However, *in vivo* studies (mostly based on magnetic resonance imaging and ultrasound) suffer from limitations in the measurement of the velocity field, due to the reduced spatial and temporal resolution of the methodology [23]. On the other hand, *in vitro* techniques do not allow the measurements of the velocity in the full field [10,19,20,24,25]. Advanced and validated *in silico* models, providing information on the 3D flow field with a detailed temporal resolution, can overcome the drawbacks of *in vivo* and *in vitro* procedures and achieve a more comprehensive understanding of the biomechanics involved in the phenomena. Specifically, high-fidelity fluid-structure interaction (FSI) simulations can enable deeper investigation of the normal, diseased and treated valve function [21,26–29]. FSI models have been used for the analysis of the aortic valve behaviour since their early development. At the end of the last century, Makhijani et al. (1997) presented a first FSI study of a pericardial bioprosthetic aortic valve in a rigid aortic root graft with physiologic sinuses [30]. Few years later, De Hart et al. (2003) employed a fictitious domain method to study the effect of FSI on the native valve behaviour for a reduced Reynolds number flow [31]. They investigated the importance of systolic functioning on the functionality of the valve. The same group analysed the mechanical and haemodynamic behaviour of a fibre-reinforced stentless aortic valve model [32]. Carmody et al. (2006) generated a finite element model of the left ventricle and performed FSI

analysis to obtain the fluid velocity profile at the aortic orifice [33]. They employed the acquired spatial and temporal velocity profiles as boundary condition for a FSI model of the aortic valve and its surrounding structures. Marom et al. (2011) developed a FSI model to analyse the end-closing phase of the valve under physiological conditions, considering the root compliance and the valve coaptation [34]. Sturla et al. (2013) simulated the function of the physiological aortic root including an asymmetric MRI-based geometry, the description of the non-linear anisotropic behaviour of the valve leaflets, and time-dependent blood pressures [35]. Sunndaram et al. (2015) proposed a comparative study between different boundary conditions applied to an FSI model of the aortic valve [36]. Wu et al. (2016) developed a FSI model of a self-expandable transcatheter aortic valve [37]. Wu et al. (2019) considered a novel immersogeometric FSI framework for the modelling and simulation of the TAVR procedure to analyse the anchoring of the prosthesis [38]. Liu et al. (2022) analysed how different flap designs affect the mechanical properties and flow field of TAVR through FSI simulations [39]. Morany et al. (2023) proposed a new FSI co-modelling framework for the haemodynamic-structural analysis of compliant aortic valves using lattice Boltzmann and finite element methods [40]. Abdi et al. (2023) analysed the potential association between different phenotypes of unicuspid aortic valves (including unicommissural and acommissural) and the occurrence of aortic diseases performing FSI simulations during systole [41]. Recently, Monteleone et al. (2024) simulated the haemodynamics in the healthy aortic valve with a new mono-physics FSI approach based on the meshless smoothed particle hydrodynamics method [42]. Yan et al. (2024) analysed different bicuspid aortic valve types employing FSI simulations and digital particle image velocimetry experiment [43]. Bornemann et al. (2024) investigated transcatheter aortic valve thrombosis through FSI simulations during systole and Lagrangian particle tracing to analyse the blood washout efficiency considering a normal and larger aorta [29]. Corso et al. (2024) compared the flow characteristics during systole in a stenotic aortic valve with those downstream of two newly designed surgical bioprosthetic aortic valves [44]. Quin et al. (2024) performed patient-specific FSI analysis of bicuspid aortic valve haemodynamics [45]. Kim et al. (2024) analysed the effect of the struts height of a bioprosthetic valve on the structural mechanics of the valve leaflet [46]. Xie et al. (2024) studied the physical mechanism behind the development of calcific aortic valve lesions [47].

In this context, Tango et al. (2018) developed a numerical model FSI-based aiming at supporting a better comprehension of the aortic valve function [27]. The analysis considers the whole cardiac cycle, including both systolic and diastolic phases (the latter is often neglected in the literature, due to the complexity in simulating leaflets coaptation) [48]. The model was first validated versus the *in vitro* study presented by Toninato et al. (2016), performed with the particle image velocimetry technique [9]. Afterwards, the validated FSI model was modified to simulate an idealised young healthy aortic valve by eliminating the experimental and methodological limitations and approximations. This model was then used by Tango et al. (2021) as a reference to identify physiological changes produced by ageing pathological condition [28].

In this study the ideal healthy native aortic valve model of Tango et al. (2018) [27] is employed as a reference to analyse numerically different post treatment configurations. Different from the above-mentioned works, SAVR and TAVR replacements are compared to the healthy native aortic valve and their impact on haemodynamics is investigated.

2. Methods

FSI analyses were performed employing the commercial explicit finite element software LS-DYNA (LSTC, Livermore, CA, USA) which is specialised in non-linear dynamic problems [49]. Thanks to its ability in modelling large deformation, advanced materials and the coupling between fluid and structure, this software is widely employed for the

analysis of heart valve fluid dynamics [35,50,51]. Moreover, LS-DYNA is included in the ISO working group list of recommended commercial software to be used for the assessment of potential thrombus formation in heart valve implants [52].

The employed FSI strategy is based on the coupling of a Lagrangian approach to model structures and a Eulerian approach to model the fluid, whilst the coupling is reached through a hybrid arbitray-Lagrangian-Eulerian (ALE) algorithm [53].

Simulations were run on an Intel Core i7 3.4 GHz workstation.

2.1. Configuration models

The idealised aortic root (see Fig. 1) was characterised by identical dimensions for the three leaflets and for the Valsalva sinuses, whose cross section was defined as an epitrochoid function [8]. The diameter at the annulus and at the sino-tubular junction (STJ) was selected equal to 25 mm, consistent to an average healthy young adult [9].

Three configuration models were considered: healthy native aortic valve (proposed in Tango et al. (2018) [27], see Fig. 1a), SAVR (Fig. 1b) and TAVR (Fig. 1c).

The leaflet geometry adopted for the healthy native aortic valve (Fig. 1a) was based on the description of the idealised healthy human aortic valve provided by Thubrikar [54].

An idealised SAVR was considered to describe the surgical bio-prosthesis configuration (Fig. 1b), where a 25 mm valve (including the stent) was placed in a supra-annular position in an aortic root with annulus and STJ diameters equal to 25 mm. Due to the presence of the stent, the leaflets diameter in the surgical prosthesis was scaled down to 23 mm, and the leaflets attachment line was positioned in the proximity of the stent base. This is the case for the most implanted bioprosthetic surgical valves, such as the Edward Lifesciences Perimount™ and Resilia™, the Medtronic Hancock™ and Avalus™ portfolios. There are also pericardial valve designs where the pericardium is wrapped around the stent (such as the Corcym Crown PRT™ or the Abbot Trifecta™ - now discontinued), which are less popular, and are not analysed in this study.

As suggested by Ducci et al. (2016) [20], the diseased native valve left in place after TAVR are idealised as a cylindrical partition positioned between the operating aortic valve and the sinuses of Valsalva (Fig. 1c).

The thicknesses of the aortic leaflet and aortic wall were considered

to be uniformly distributed, imposing a value of 0.5 mm [55–57] and 3 mm [35], respectively.

2.2. Mesh

ICEM 17.0 (ANSYS, Inc., Canonsburg, PA, USA) was employed to mesh fluid and structure domains. In particular, the fluid domain was discretised with a structured mesh of 113520 8-noded hexahedral Eulerian elements with a characteristic dimension of 1 mm.

All structural components, including the aortic root, the stent, the valve leaflets and the partition, were modelled as shell and discretised with 4-noded Belytschko-Tsay elements [49] (9960 for the aortic root, 6852 for the SAVR stent, 6564 for the leaflets, and 1836 for the partition).

The mesh convergence analysis of the employed model is described in detail in the supplementary material of Tango et al. (2018) [27].

2.3. Material properties

The native aortic root is made of soft tissues, primarily composed of networks of collagen and elastin fibres embedded within an amorphous matrix containing proteoglycans. This microarchitecture governs the nonlinear stress-strain response, characterised by an initial plateau followed by increased stiffness due to progressive recruitment of the wavy collagen fibres. The specific amount and distribution of these components determine the local material response, with the overall behaviour achieved by a combination of layers with different compositions.

This is the case of the native aortic leaflets, which are composed of three distinct layers: the fibrosa (on the aortic side), the ventricularis (on the ventricular side), and the spongiosa (intermediate dampening layer). This complex arrangement exhibits non-uniform distribution across the leaflet area, with thickened regions at the free margins defining a central bulge (nodule of Arantius) and two crescent-shaped apposition regions (lunulae) [58]. Despite this complexity, the fibrosa layer, which covers the entire leaflet surface and consists of a dense network of circumferentially oriented type I collagen fibres, is the main contributor to the mechanical response of the tissue [59]. Due to the demonstrated ability of simplified models to accurately replicate aortic valve dynamics [27], in this study native leaflets were modelled as a single homogeneous and isotropic layer. This assumption is particularly convenient for the
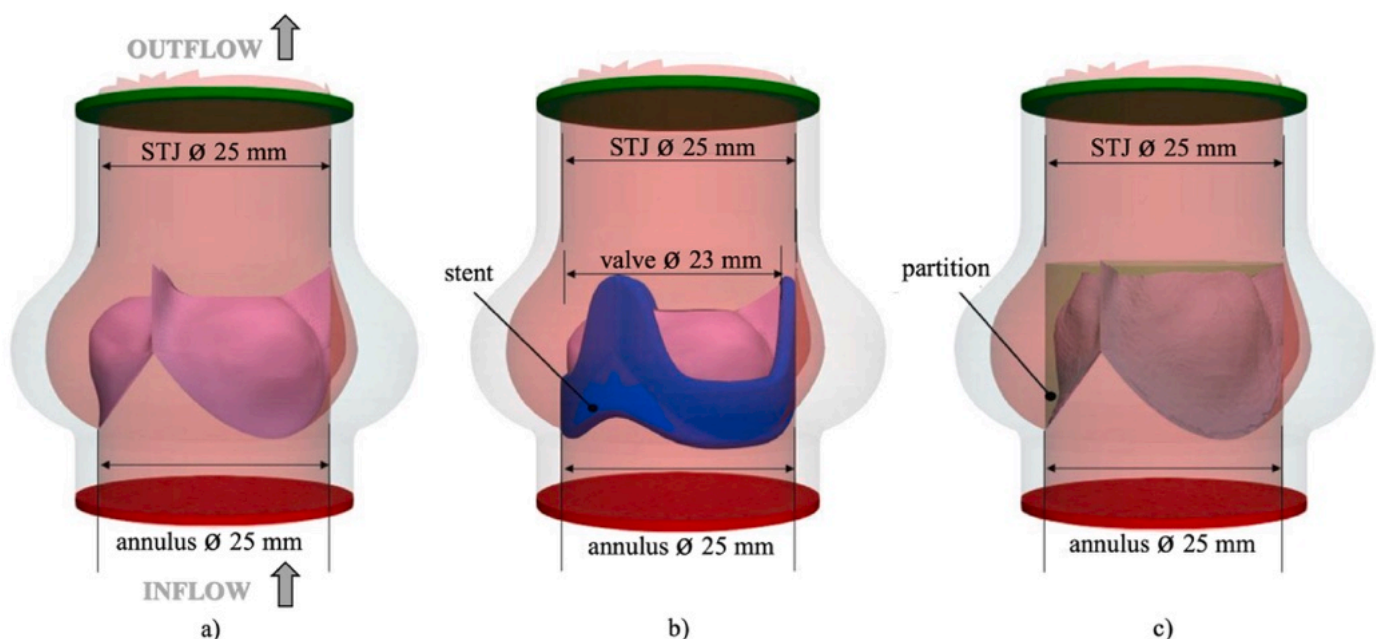

Fig. 1. Configuration models. a) Healthy native aortic valve proposed by Tango et al. (2018) [27] [27]; b) SAVR and c) TAVR.

modelling of the SAVR and TAVR model. In fact, the leaflets of these valves are typically obtained from the fibrosa layer of xenograft parietal pericardium (commonly bovine or swine), which can be regarded as a single, nearly homogeneous sheet of multidirectional bundles of collagen and elastin fibres [60]. In general, healthy human aortic valve leaflets and xenograft pericardium exhibit a similar nonlinear hyperelastic incompressible stress-strain response [61], which was described using an Ogden's constitutive model, whose material characteristic constants were based on the experimental results from Bozkurt et al. (2017) [62] (reported in Table 1). A density, ρ_s, equal to 1100 kg/m³, typical of biological tissues [63], was set for the material.

The ascending aorta is classified as an elastic artery (non-muscular), and is characterised by a three-layer structure, comprising the intima (thin inner layer), the media (middle layer), and the adventitia (outer layer). In healthy conditions, the mechanical response of the root is mostly controlled by the media layer, which consists of a complex three-dimensional arrangement of smooth muscle cells and elastin and collagen fibres, helically wound along the root axis. As for the leaflets, this microarchitecture produces a nonlinear stress–strain response, which is clearly observed in *ex vivo* mechanical testing, where the arterial tissue is loaded from the unloaded configuration (which does not typically correspond to the unstressed configuration) [64]. However, under physiological operating conditions, the root is constantly subjected to a pressure commonly larger than 80 mmHg, which maintains the material at stress levels above the initial plateau and makes the assumption of linear behaviour acceptable [65]. Hence, the aortic wall was modelled as linearly elastic. In the case of the healthy and surgical models, the value of the Young's modulus, E_c, was selected to match the vessel compliance of a normal healthy ascending aorta, coherently to the international standard ISO 5840 [66]. For the TAVR model, the Young's modulus, E_s, was set to achieve a low compliance [66], which is more representative of the patients undergoing the procedure. To model the near incompressibility of the material, a Poisson's ratio $\nu = 0.45$ was used for both conditions. The values of the Young's moduli and Poisson's ratio used to describe the ascending aorta response are reported in Table 1.

The fluid was modelled as incompressible and Newtonian, with a dynamic viscosity $\mu_f = 4.0 \times 10^{-3}$ Pa • s and density $\rho_f = 1060$ kg/m³.

2.4. Boundary conditions

The boundary conditions applied in the FSI simulations are summarised in Fig. 2. These, representing a combination of physiological flow velocity and pressure differences, are based on the work of Tango et al. (2018) [27].

Specifically, an aortic pressure waveform oscillating between 80 mmHg (diastolic) and 120 mmHg (systolic) was imposed at the outflow section (dotted black line in Fig. 2).

At the inflow section, the velocity flow waveform measured by Toninato et al. (2016) [9] was applied during systole, uniformly distributed over the inlet cross section. During diastole, the velocity profile was replaced by the ventricular pressure waveform (dashed black line in Fig. 2) measured from the same *in vitro* study [9]. This allows to best simulate the closing dynamics, where the closing leakage occurs as result of the transvalvular pressure difference [36].

3. Results and discussion

The biomechanics of surgical and transcatheter replacement procedures were investigated and compared against the idealised healthy native valve [27]. In particular, the kinematics, flow velocity, pressure field, effective orifice area and transvalvular pressure gradient were analysed throughout the cardiac cycle for the different configurations. This allowed to investigate how existing treatments may affect the aortic valve performance.

3.1. Valve kinematics

Valve kinematics is a key parameter to evaluate the performance of the valve during the opening and closing phases. This was analysed by measuring the radial displacement of the central node at the leaflets edge (given the 120° symmetry of the valve model, analysis of a single leaflet is representative of the entire valve). Diagrams of the radial displacement for the healthy native and treated configurations during the whole cardiac cycle are represented in Fig. 3.

As recommended in the international standards ISO 5840 [66], the valve opening and closing times were used to analyse the valve kinematics during the cardiac cycle, defined and quantified as follows [67]:

- *valve opening time*, calculated as the time interval between the beginning of the leaflets opening and the full valve opening (interval t_1-t_2 in Fig. 3).
- *valve closing time*, calculated as the time interval between beginning of the valve closure and the complete valve closure (interval t_3-t_4 in Fig. 3).
- *ejection time*, calculated as the total time interval between the beginning of the valve opening and the complete valve closure (interval t_1-t_4 in Fig. 3).

The calculated *opening, closing* and *ejection times* are summarised in Table 2. Additionally, to provide a more comprehensive view of the leaflets kinematics, the following time references are defined:

- *slow reduction in the opening* as systole progresses towards its end (interval t_2-t_3 in Fig. 3);
- t_1', positioned at the centre of interval t_1-t_2;
- t_2', positioned at the centre of interval t_2-t_3 (slow closure);
- t_3', positioned at the centre of interval t_3-t_4.

Results for the healthy native model are coherent with other *in vivo* [68] and numerical studies [67,69], with the valve opening and closing times equal to about 50 ms. The SAVR configuration is characterised by a slower valve dynamics than the healthy native and TAVR configurations, with substantially longer valve opening and closing times, lasting 80 and 90 ms, respectively (these are 60 % and 80 % larger, respectively, than for the healthy native configuration). In particular, the opening phase begins earlier in the cardiac cycle than the other configurations, but terminates later (see Fig. 3).

The closing phase begins at the same time as for the TAVR, but completes significantly later. The TAVR configuration presents opening
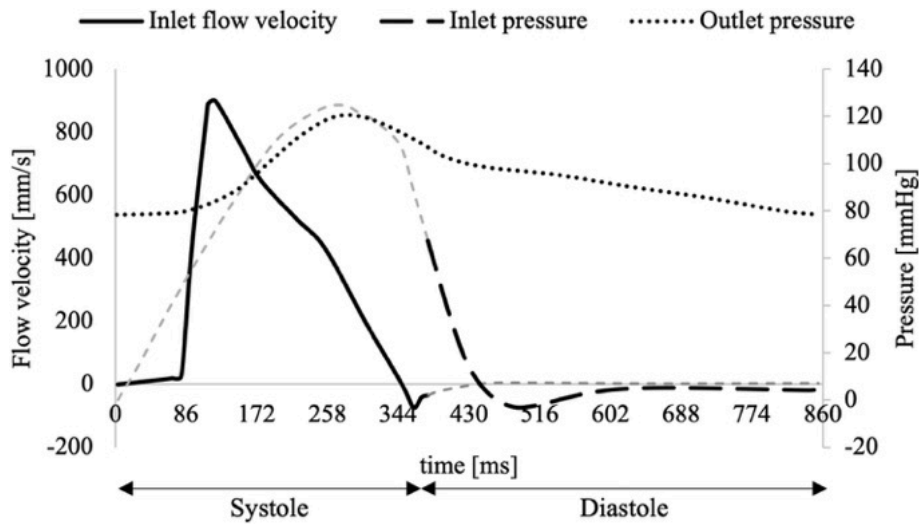
Table 1

Constitutive/rheological models and parameters defined for the materials used in the simulations and for blood.

Component	Model	Coefficients and properties
Leaflets	hyperelastic incompressible: Ogden's formulation	Equation: $W = \sum_{p=1}^{N} \frac{\mu_p}{\alpha_p}(\lambda_1^{\alpha_p} + \lambda_2^{\alpha_p} + \lambda_3^{\alpha_p} - 3)$; where *W is the strain energy, $\lambda_{1,2,3}$ are the principal stretches, μ and N are material characteristic constants* Parameters: $\mu_1 = 7.6 \times 10^{-6}$ MPa; $\mu_2 = 5.7 \times 10^{-6}$ MPa $\alpha_1 = \alpha_2 = 26.26$; $\rho_s = 1100$ kg/m³
Ascending aorta	Linear elastic	Young's moduli: $E_c = 0.92$ MPa (healthy native and SAVR) $E_s = 3.25$ MPa (TAVR) Poisson's ratio: $\nu = 0.45$ Density: $\rho_f = 1060$ kg/m³
Stent/ partition	Rigid	–
Blood	incompressible Newtonian fluid	Dynamic viscosity: $\mu_f = 4.0 \times 10^{-3}$ Pa • s Density: $\rho_f = 1060$ kg/m³.

Fig. 2. *Boundary conditions-velocity and pressure waveforms, from Tango* et al. *(2018)* [27]. *The grey lines are the extension of the inflow velocity and pressure curves not imposed in the simulations.*
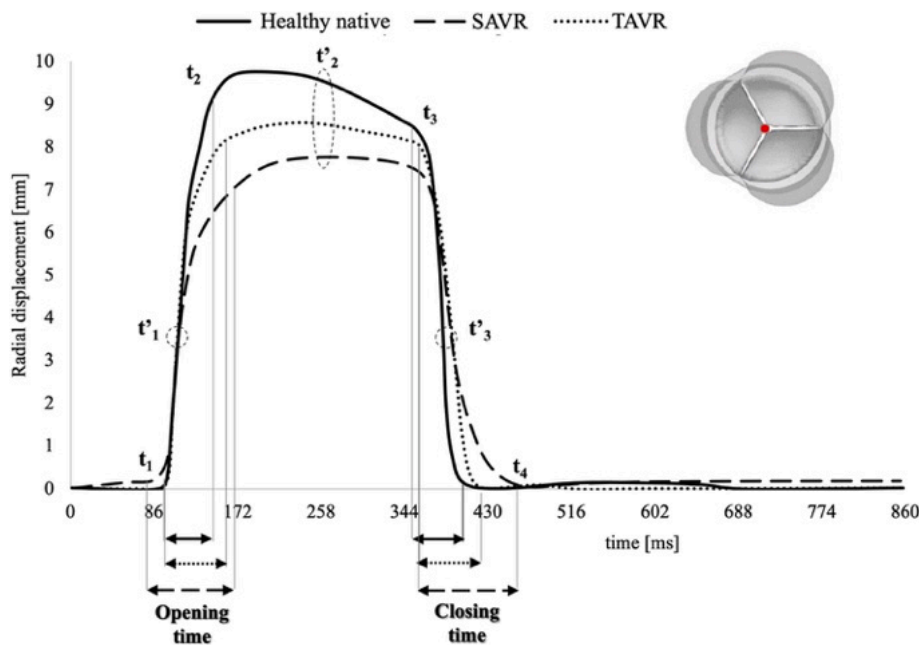

Fig. 3. Leaflets kinematics in healthy native (black continuous line), SAVR (black dashed line) and TAVR (black dotted line) models. The red point on the leaflet shows the location of the node where the displacement was tracked for all configurations. t_1: initiation of the valve opening, t_1': lying in the middle of t_1-t_2, t_2: full opening, t_2' lying in the middle of the t_2-t_3, t_3: initiation of the valve closure, and t_3' lying in the middle of the t_3-t_4 and t_4: full closing.

Table 2
Valve opening, closure and ejection times for healthy native, SAVR and TAVR models.

Configuration	Opening time [ms]	Closing Time [ms]	Ejection time [ms]
Healthy native	50	50	310
SAVR	80 (+60 %)	90 (+80 %)	362 (+16 %)
TAVR	60 (+20 %)	70 (+40 %)	330 (+6 %)

and closing times closer to the healthy native valve and equal to 60 ms and 70 ms, respectively (20 % and 40 % longer, respectively, than for the healthy native configuration). The slower response of the SAVR and TAVR configurations is associated with extended ejection times, respectively 16 % and 6 % longer than for the healthy native case (see Table 2). The healthy native valve exhibits wider opening during systole,

with the leaflets reaching a maximum radial displacement of 10.0 mm at the systolic peak. This value reduces to 8.0 mm (20 % lower) for the SAVR configuration and 8.8 mm (12 % lower) for the TAVR. However, it is worth to mention that the configuration when the maximum radial displacement is achieved does not necessarily correspond to a fully open valve configuration, but may occur before the end of the opening phase. In fact, during opening, the centre of the leaflet free edge tends to expand earlier than the leaflet belly, to radial positions larger than those taken when the whole leaflet has reached the open shape [28].

A snapshot of valves from the outflow, acquired at time instants t_1, t_1', t_2, t_2', t_3, t_3' and t_4, is reported Fig. 4. Analysis of the images confirms a reduction in leaflets expansion during systole. This is expected in the case of SAVR, since leaflets were scaled down to account for the stent thickness. However, also the general shape of the fully open configuration appears very different from the healthy native case, with the
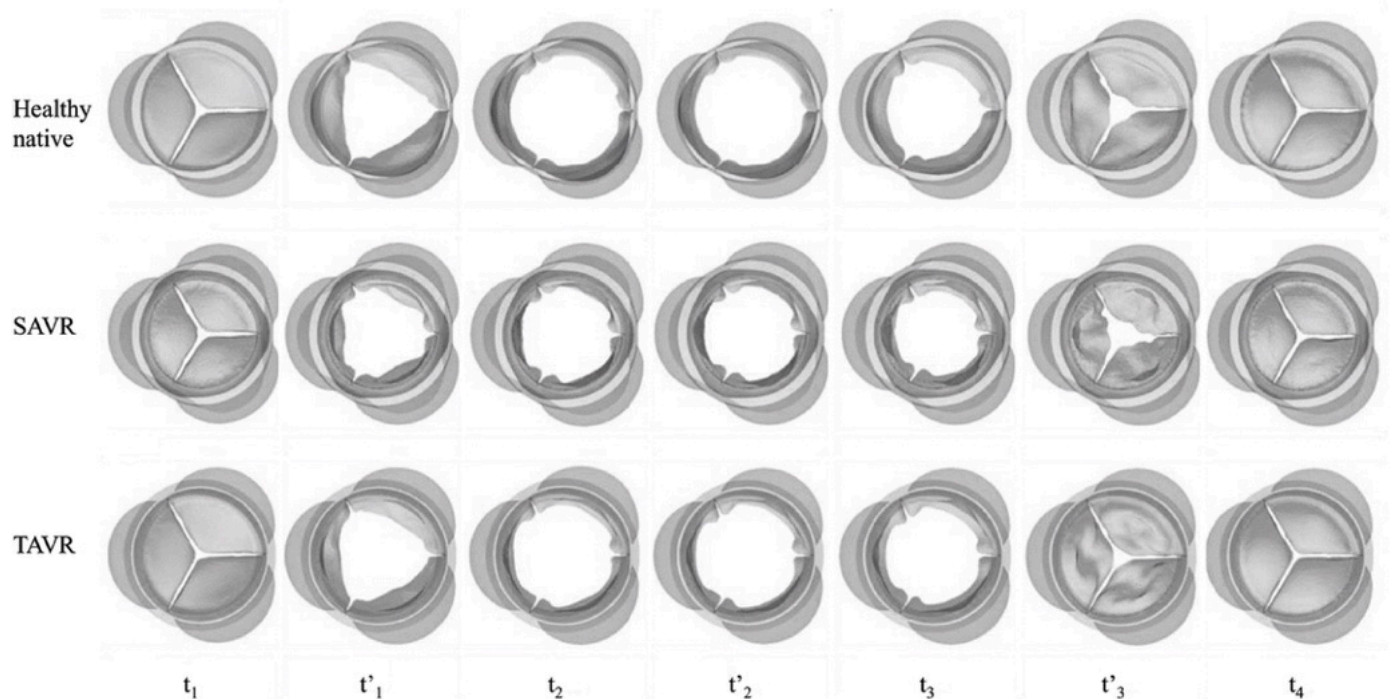
Fig. 4. Valve top view for healthy native, SAVR and TAVR models at the instants used for the calculation of the valvular kinematics parameters.

leaflet belly unable to expand beyond the inner wall of the stent. This distorted configuration, characterised by larger snap through energy, may be the reason for the stiffer behaviour observed also during closing.

In the case of the TAVR model, despite leaflets were kept identical to the healthy native model, the presence of the native leaflets and stent limits their ability to expand into the sinuses, resulting in restricted opened configurations, compared to the healthy native case.

3.2. Flow velocity

The fluid dynamics and global flow parameters were investigated for all models, comparing the vortical behaviour and haemodynamics obtained for the SAVR and TAVR cases against the healthy native valve [27]. Full field maps of the fluid velocity are shown for a sagittal cross section bisecting one of the sinuses and the opposite commissure (Fig. 5). Maps are provided at selected instants of the cardiac cycle, which include: the systolic peak (A); the end of systole (B); the first leaflets coaptation in the early diastole (C); and a fully closed configuration in the middle of diastole (D). To better visualise the vortical structures that form during the cycle, Fig. 6 reports the streamlines obtained from line integral convolution for the most indicative instants (A and C). Moreover, velocity maps are also shown for a transversal cross section at the level of the maximum diameter of the Valsalva sinuses (Fig. 7). The axial velocity profiles at the STJ (indicated as a dashed white line in Fig. 5) is provided in Fig. 8 for the healthy native (continuous line in Fig. 8), SAVR (dashed line in Fig. 8) and TAVR (dotted line in Fig. 8) models.

The SAVR model shows a series of large vortices and counter vortices developing in the Valsalva sinus during the opening stage and occupying the region for the whole systolic duration. These mostly develop between the leaflets and the arterial wall, and are much more evident than for the other cases (see instant A in Figs. 5 and 6). In fact, coherently with the hydrodynamics reported in *in vitro* studies performed on SAVRs [9,19], the smaller leaflets and stent-limited expansion result in a large chamber between the valve and the sinus wall, that supports and sustains a system of large vortices and counter vortices. This work reveals that these vortical structures are highly three dimensional, and large

couples of opposing vortices can be observed in the transversal plane of each sinus (see instant A in Fig. 7). These are not evident in the healthy native case. A small vortex is also observed inside the small concavity that forms in the open leaflet (see instant A in Fig. 6). This is smaller than for the healthy native leaflet, which bulges into the sinus, promoting the formation of three-dimensional recirculation observable in both the sagittal and transversal cross sections. The stent thickness also produces a larger recirculation above the commissure, compared to the other models. The combination of a geometrically smaller annulus and large recirculations at the valve outflow causes a marked narrowing of the systolic jet, which is evident looking at the velocity profile at the STJ represented in Fig. 8a and b. This contraction has the effect of increasing in the systolic blood velocities, whose peak is equal to 2.1 m/s, compared to only 1.3 m/s estimated for the healthy native case. The development of a large vortex above the stent post and higher velocities in the systolic flow are also observed in the experimental work from Toninato et al. (2016) [9] for all surgical valve configurations. This study suggests that the presence of systolic vortices observed in the sinuses after SAVR [9,70,71] is not associated with healthy operating conditions, but rather with a stenotic dynamics due to geometric mismatch or other non-physiological causes, such as the constricting presence of a supporting stent, as in the presented post treatment cases. It also highlights that experimental settings based on the inclusion of a bioprosthesis to mimic the native aortic valve cannot be representative of realistic healthy native conditions. During early diastole (instant C in Figs. 5 and 6) the presence of the stent channels the returning flow, so that the leaflets base receives an axial rather than centripetal flow. The stent also drives away from the leaflets the location where the washing vortex initially forms. This diastolic recirculation, which in the healthy native configuration has a three dimensional pattern which contributes to the smooth valve closure, looses its spatial features with the surgical bioprosthesis and reaches the leaflets of only once it has significantly expanded, at a later stage of the diastole (see instants C and D in Figs. 5 and 7). This justifies the delayed valve closure observed for this model. It should be noted that the small reverse flow jet evident in all models at late diastole (instant C in Fig. 6) is a common artefact of the FSI methodology, which requires the inclusion of a small gap (0.1 mm in this
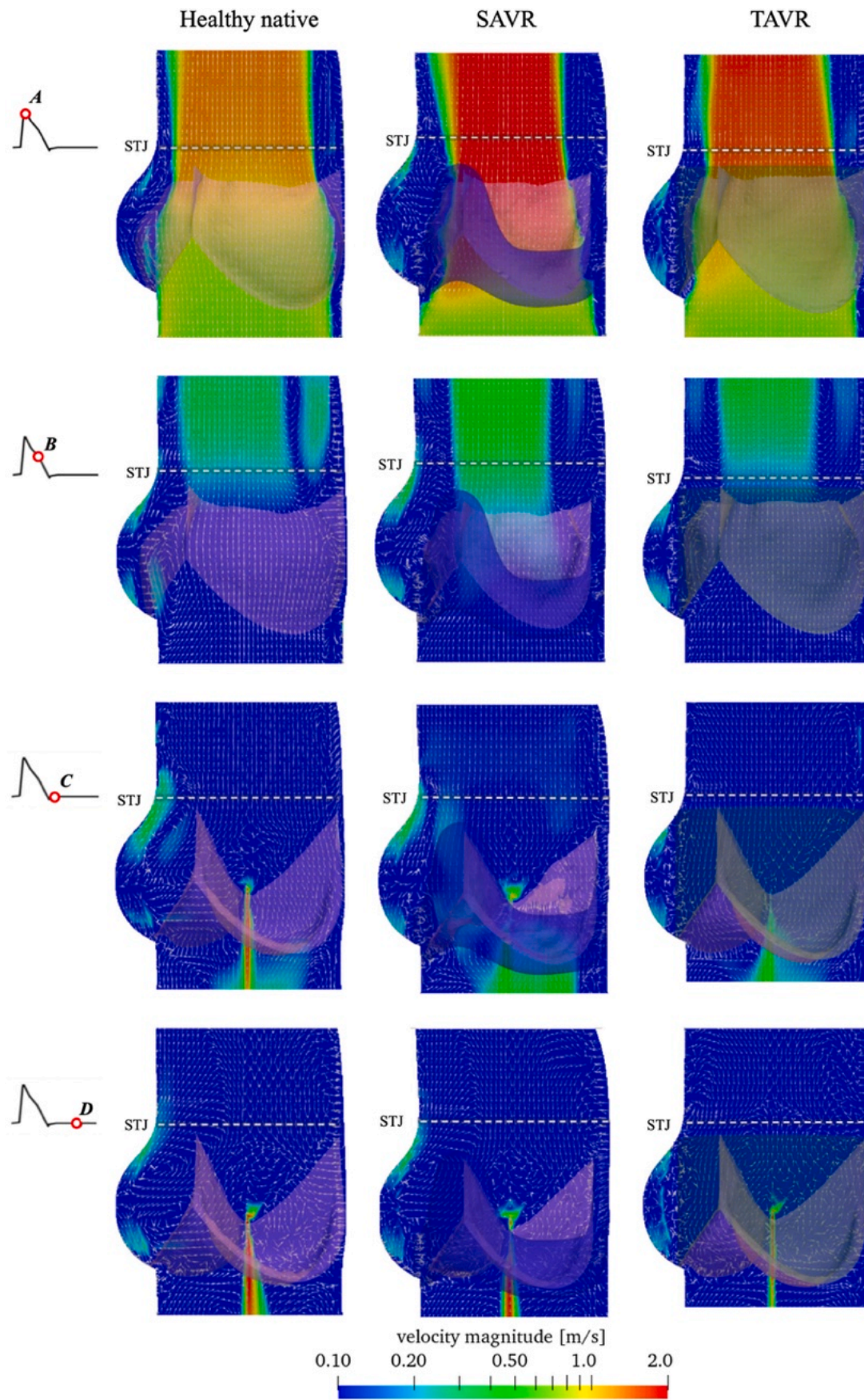
Fig. 5. Velocity contour maps and vectors (in white) in a longitudinal cross-section for healthy native, SAVR and TAVR models. The dashed line highlighted the STJ.
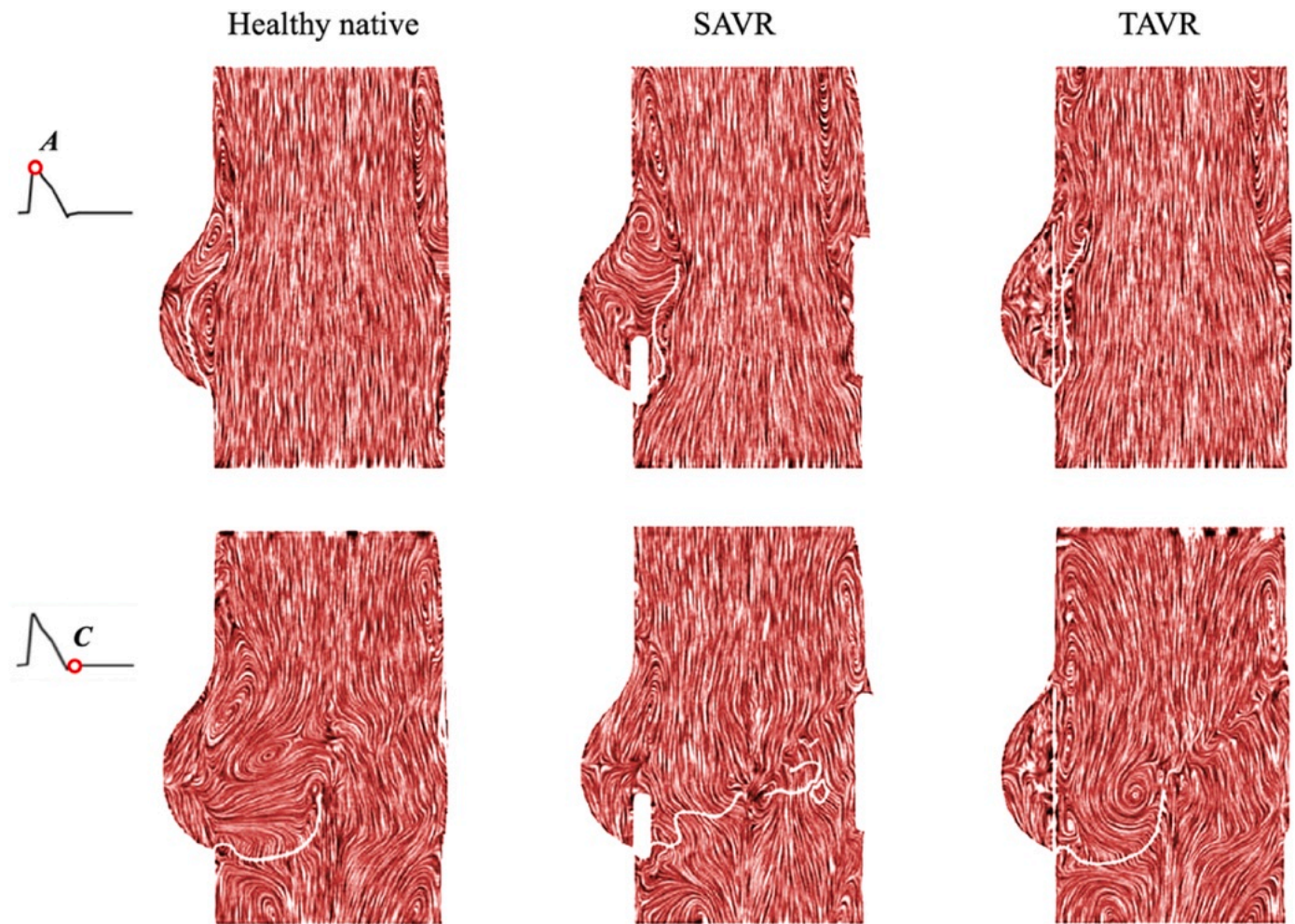
Fig. 6. Velocity maps and streamlines (visualised using line integral convolution, LIC) at leaflets opening (systolic peak, instant A) and closure profile (early diastole, instant C) obtained for healthy native, SAVR and TAVR models.

study) between the leaflets of the closed valve configuration to allow the valve to open [28].

In the case of the TAVR model, no structured vortices can be observed within the Valsalva sinuses throughout the cardiac cycle. This is due to the presence of the partition, which reduces the available space in the cavity between the expanded native leaflet/stent and the sinus wall. However, contrary to what observed in previous *in vitro* studies [19,20,72] that indicate persistent blood stasis in the region, a stronger flow activity is observed. This is due to the fact that, being the root modelled as a compliant vessel, the sinuses undergo cyclic expansion/-contraction under the effect of the pressure changes, producing a pumping action. In the case of elderly patients with stiffer root this effect is expected to reduce, increasing blood stasis at the base of the sinuses. Vortices inside the open leaflets concavity and around the central jet become evident only later in the systole (instant B in Fig. 5). The flow distribution downstream the valve is characterised by a mostly axial symmetrical jet, slightly narrower than that of the healthy native model (see Fig. 8a and b), due to the inability of the prosthetic leaflets to expand beyond the cylindrical shape of the native leaflets/stent partition, as described in *in vitro* studies on TAVR configurations [20]. This produces a peak in the maximum systolic velocity measured at the STJ equal to 1.6 m/s, which is to some degree larger than for the healthy native case, but substantially lower than for SAVR (see instant *A* in Fig. 5). Globally, apart of the stagnation region in the sinuses, the valve dynamics features at systole appear more physiological than for the SAVR model (see instants A and B in Figs. 5–7). Large recirculations in

proximity to the leaflets develop in the early stage of diastole (instant C in Fig. 5) and then split into multiple smaller vortices as diastole progresses (instant D in Figs. 5 and 6). Closing is prompter compared to the surgical bioprosthesis, although no relevant vortical structures can be observed during diastole, as evident from the very reduced variations in the velocity profile observable in Fig. 8c and d. The partition, in fact, channels the flow, forcing leaflets to close under the action of a mostly axial flow (instants C and D in Figs. 5 and 7).

3.3. Pressure maps, effective orifice area (EOA) and transvalvular pressure gradient

The pressure contour maps determined for all models at the selected instants are reported in Fig. 9 (for the sagittal plane). The main differences are observed at the peak systole (instant *A* in Fig. 9), whilst the pressure distributions in the other time frames are mostly coherent with the healthy native pressure maps (see instants *B*, *C* and *D* in Fig. 9). The valve performance indicators computed for the native and treated cases are summarised in Table 3.

In the early systole, the more restrictive profile of the SAVR model produces a higher ventricular pressure compared to the healthy native case, leading to an increased ΔP (13.1 mmHg vs. 4.6 mmHg). This increase in pressure loss is reflected in the estimated EOA, which is equal to 1.7 cm^2. This value, which is over 40 % smaller than the value obtained for the healthy native valve (2.9 cm^2), is coherent with the data obtained from doppler echocardiographic evaluation on bioprosthetic
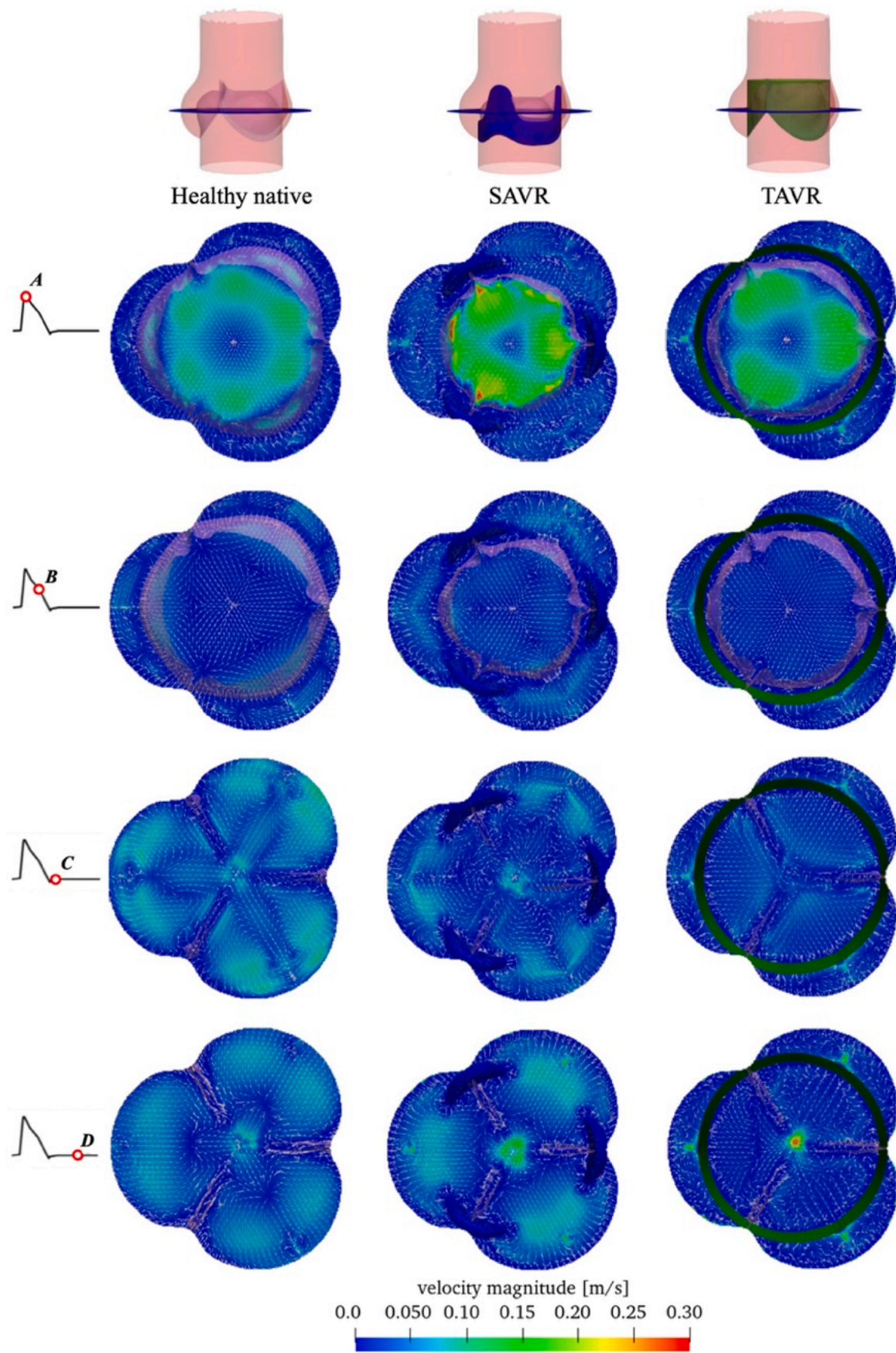
Fig. 7. Velocity contour maps, vectors (in white) in a transversal cross-section at the valve orifice for healthy native, SAVR and TAVR models.
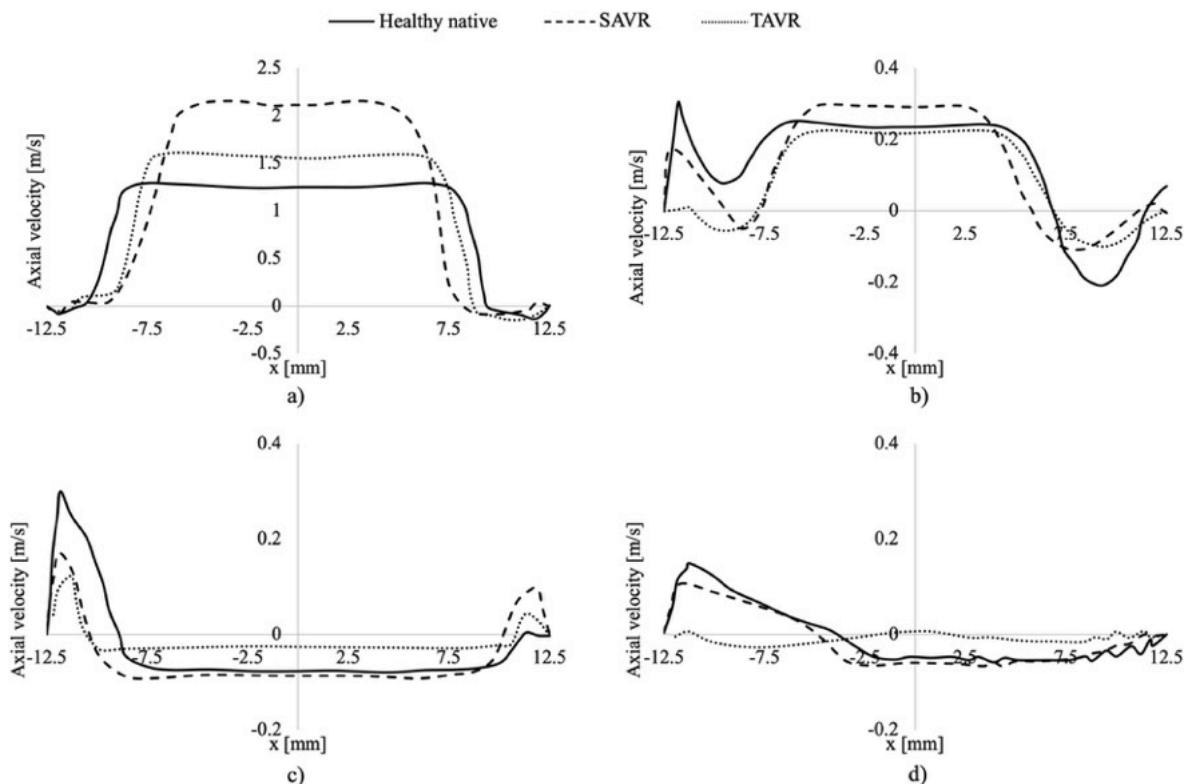
Fig. 8. Comparison of the velocity profiles extracted at the STJ level for healthy native (continuous line), SAVR (dashed line) and TAVR (dotted line) models. a) instant A; b) instant B; c) instant C and d) instant D.

valve of the same size [73] and with other works related to SAVR [74, 75]. For the SAVR model, the region of low pressure into the sinuses observed for the other cases is much less evident. This is generated by the Venturi effect associated with the central jet, and it has been suggested by Tango et al. [27,28] as a mechanism enhancing the performance of the healthy native valve. In fact, at the systolic peak, it generates a suction that drives the leaflets deeper into the sinuses, widening their opening and resulting in superior hydrodynamic valve performance.

It is worth noticing that the region of reduced pressure acts at the locations where the coronary ostia are normally expected (although they are not modelled in the present study).

TAVR pressure distributions appear closer to those of the healthy native valve, although still associated with transvalvular mean systolic pressure drops over 50 % higher (7.2 mmHg). This is correlated with an EOA of 2.3 cm^2, which is just 21 % smaller than in the healthy native case. This finding agrees with data reported by other works focused on TAVR devices [76,77]. Interestingly, the reduced gap between the main aortic lumen and the sinuses, due to the presence of the partition, amplifies the pressure reduction into the leaflets compared to the healthy native model (see instant A in Fig. 9). Even though this suction does not act on the prosthetic leaflets, which are radially constrained by the barrier, might have some effect on the coronary flow.

The advantage of TAVR over SAVR in terms of ΔP and EOA are coherent with the clinical evidence, with similar valve performance results reported between transcatheter valve types [78–80].

A further key parameter to evaluate the impact of valve function on myocardial performance is the energy loss. This is calculated as the integral of the product of the flow rate and the transvalvular pressure over a relevant flow interval [81]. In particular, the forward energy loss, calculated during ejection, is mostly associated with kinetic energy dissipation due to viscous eddies. The closing energy loss is mostly associated with the volume of blood returning into the ventricle as effect of the dynamics of valve closure, that must be re-pumped through the

valve requiring additional work. The energy loss calculated with the different models during forward flow and closing is summarised in Table 4.

As expected, forward and closing energy values for the healthy native model are substantially lower than for the treated configurations. The alterations in the systolic flow produced by the presence of the surgical valve considerably increase the energy lost during forward flow, which is nearly 3 times larger than in healthy native conditions. Similarly, the delayed closing dynamics more than doubles the energy absorbed during valve closure (125.7 % larger than for the native valve). This phase, though, has a lower contribution in the overall energetic loss, which globally results 162.4 % larger than for the native valve.

In the case of the TAVR, the more physiological systolic phase is associated with much lower forward flow energy loss, about 50 % higher than in the healthy native valve. Closure losses are practically identical to those in the SAVR model, despite the very different valve dynamics. Globally, the TAVR model halves the losses compared to SAVR (these are 76.4 % larger than in the native valve). However, it is essential to consider that the model is highly idealised, and does not describe the paravalvular leakage, that represents a common complication after TAVR and reduces substantially the performance of transcatheter valves.

3.4. Potential for blood damage

Blood damage depends on a number of factors, including the hydrodynamic state as well as tissue wall injury, presence of foreign materials and altered blood biochemistry [52,82]. In terms of hydrodynamics, fluid environments presenting elevated shear stresses and flow separation areas may lead to haemolysis or blood activation [83], whereas regions characterised by slow flow velocities are prone to platelet aggregation and thrombus deposition [6,10,21].

Fluid shear stress maps are shown in Fig. 10. In all configurations, higher values of shear stress were detected at the systolic peak and valve
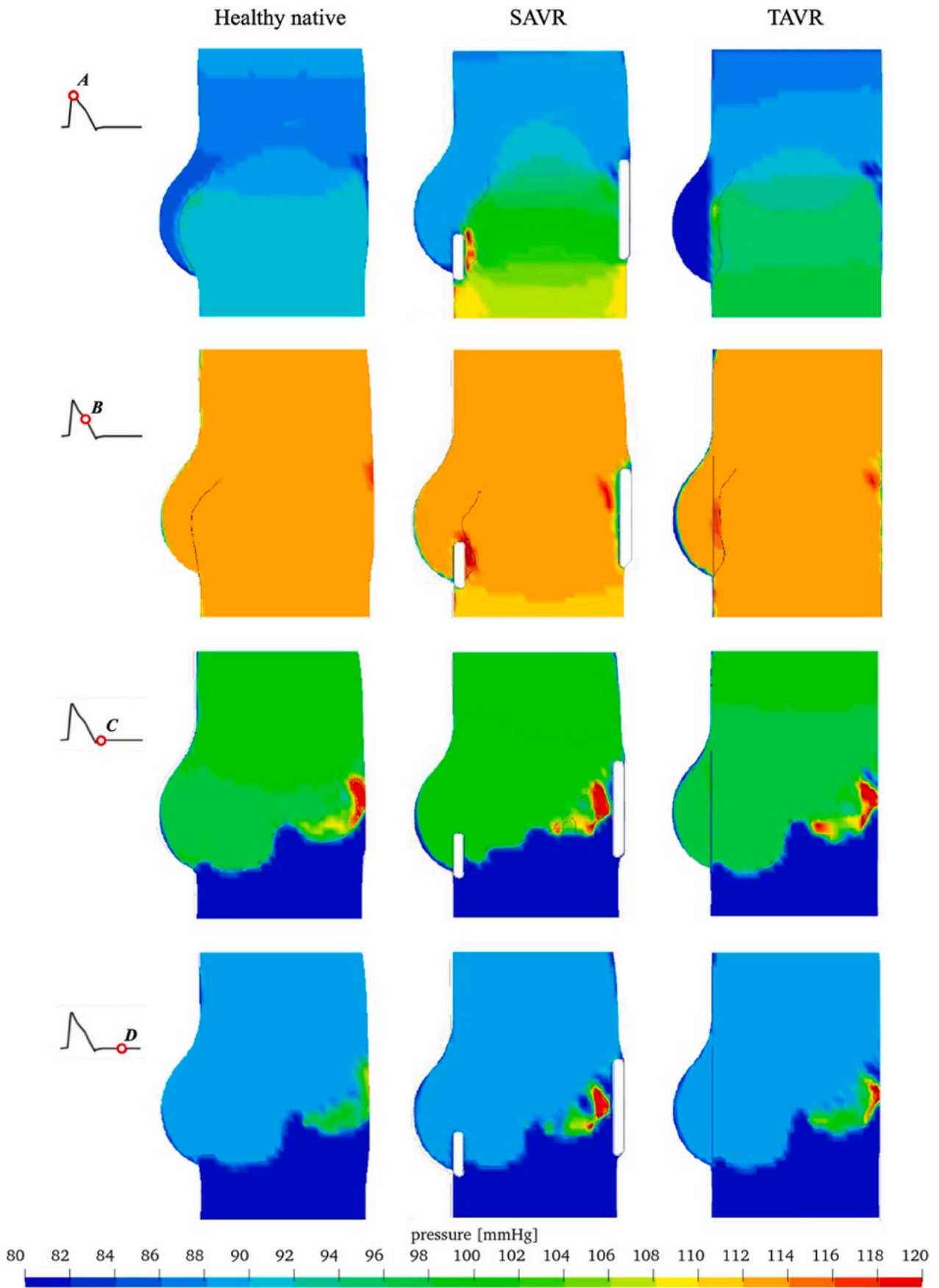
Fig. 9. Pressure contour maps for healthy native, SAVR and TAVR models.

Table 3

Transvalvular pressure drop (ΔP) and EOA values for healthy native, SAVR and TAVR models.

Valve configuration	ΔP [mmHg]	EOA [cm^2]
Healthy native	4. 6	2.9
SAVR	13.1 (+185 %)	1.7 (−41 %)
TAVR	7.2 (+57 %)	2.3 (−21 %)

Table 4

Energy loss values for healthy native, SAVR and TAVR models.

Valve configuration	Forward energy loss [mJ]	Closing energy loss [mJ]	Total energy loss [mJ]
Healthy native	67.7	36.9	104.6
SAVR	191.1 (+182.3 %)	83.3 (+125.7 %)	274.4 (+162.4 %)
TAVR	101.6 (+50.1 %)	82.9 (+124.6 %)	184.5 (+76.4 %)

closure. During systole, high shear stress regions are focused in the proximity of the leaflets edges, and are associated with flow separation phenomena. During closing, they are concentrated at the central gap where blood regurgitates into the ventricle. Peak values are similar for all models (between 9.2 and 9.5 Pa), remaining one order of magnitude below the haemolytic threshold identified by Leverett et al. [84], which is in the range of 150 Pa. Hence, the observed departure from the physiological hydrodynamics is not expected to result into haemolytic blood damage. The levels of shear stress observed into the sinuses appear of similar magnitude for all models. This confirms that, if the aortic root retains some compliance, also the TAVR configuration appears to provide some washout action, reducing the risk of clot formation. This also indicates that *in vitro* models should mimic the vessel compliance to provide realistic information on the potential blood damage.

In order to verify the risk of thrombosis on the valve cusps, the wall shear stress (WSS) magnitude acting on leaflets of the different models during the cardiac cycle was analysed. This corresponds to the frictional force exerted by the blood flow on the leaflets and, therefore, to the changes of fluid velocity vector in the proximity of their surface. WSS contour plots of the valves of each model, observed from the outflow, are represented in Fig. 11 for the selected time instants (highlighted in the cardiac cycle graph with red full circles). Values keep well below the haemolytic threshold for all cases. Stents of the surgical and transcatheter valve models are exposed to very low WSS levels for the whole cardiac cycle. Moreover, TAVR leaflets show a similar distribution to the healthy native valve, with exception of the region where they are attached to the stent, which experiences very reduced levels of WSS for most of the cycle. Subclinical leaflet thrombosis of bioprosthetic aortic valves is a common complication, which often causes reduced leaflet motion [17,85] with consequent increase of ΔP or aortic insufficiency [86]. Although it is also observed in surgical valves, it is far more frequent in transcatheter aortic valves [85,87,88] where it is observed in up to 10 %–15 % of patients [89]. In particular, as described in the literature, a higher incidence of silent ischemic lesions and dementia is reported after TAVR [16,18]. Thrombus primarily originates on the aortic side of the valve, between the leaflet and the stent, mostly at the base of the leaflets [17], although thrombus on the aortic surface near the commissures is also reported [86]. These locations are coherent with the regions of low WSS indicated above, suggesting that blood stagnation may have a role in the complication. The phenomenon that leads to the triggering of thrombosis in TAVR, not captured by FSI analysis, may be related to tissue fissuring and endothelial denudation caused by the impact of the leaflets on the wall, which provides additional nests for red cells and platelets [90].

4. Limitations

Some limitations and assumptions of this study should be highlighted. In particular, to better identify the fundamental mechanisms driving the analysed phenomena and achieve a clear interpretation of the results, idealised morphologies were used for the native and prosthetic leaflets, the ascending aorta, the stent and partition. Moreover, the presence of coronary arteries and associated flows was not included.

In terms of material properties, all soft tissues were modelled as a single homogeneous and isotropic layer, disregarding their composite anisotropic multilayer and inhomogeneous nature. To better isolate the key factors altering the flow, identical material properties were used for the native and prosthetic leaflets. Also, based on the limited amplitude and relatively large mean of the loading pressure experienced under physiological conditions by the ascending aorta [65], its wall material was assumed to follow ideal Hookean behaviour. The flexibility of the stents, which strongly depends on the specific valve size and design, was neglected, considering the component perfectly rigid. Still, the ability of these simplifications to captures the essential features of aortic valve haemodynamics was previously validated through *in vitro* PIV studies [27].

Regarding the fluid model, considering the large size of the vessels and the high shear rates, blood was assumed to behave as a Newtonian incompressible fluid, neglecting its complex rheological response [91]. Paravalvular leakage was neglected in this study. This is a well-known complication following TAVR, that varies from patient to patient and can reduce significantly the performance of transcatheter valves during systole. However, as mentioned previously, the aim of this work is to isolate the alterations introduced by each factor by idealising the problem to improve comparison between healthy and treated models. It needs to be observed that paravalvular leakage has now been strongly mitigated in the new generation of TAVR devices [87–89].

The described simplifications allow for efficient simulations and a clearer interpretation of results, with the goal to establish a baseline understanding of the impact of valve replacement on haemodynamics. However, they make the models unable to capture all the complexities of a patient-specific system, where the anatomies are irregular and the components change in material properties, design, size and position, possibly influencing the flow patterns. Still, the essential features of the flow dynamics captured by the study are in general agreement with the flow features observed from experimental and clinical works performed on different setups and with different prosthetic devices [9,17,19,20,27, 78–80,86,92,93]. Hence, the insights gained from the model provides a valid foundation for future research and for the development of improved valve designs and surgical techniques.

5. Conclusions

This computational study investigates the unphysiological changes produced by surgical and transcatheter aortic valve replacements, and how these can disrupt normal haemodynamics and lead to clinical complications. Both, surgical and transcatheter replacements appear to alter substantially the fluid dynamics of the region, hindering the function of the Valsalva's sinuses to support the opening and closing leaflets dynamics. In the case of surgical valves, the presence of a thick stent results in a faster systolic jet and reduced systolic efficiency. Transcatheter valves, on the other hand, can achieve hydrodynamic performance closer to the healthy native valve, but substantially alter the valve dynamics and the blood flow in the sinuses and at the prosthetic leaflets attachment, potentially promoting ischaemic complications. Hence, current prosthetic heart valves, whether surgical or transcatheter, impact on the valve well-functioning, introducing potential sources for post-procedural complications in the long term.

The provided insights into the mechanisms underlying normal and abnormal valve function supports a better awareness of the potential impact of the replacement procedures on patient outcomes, and guide
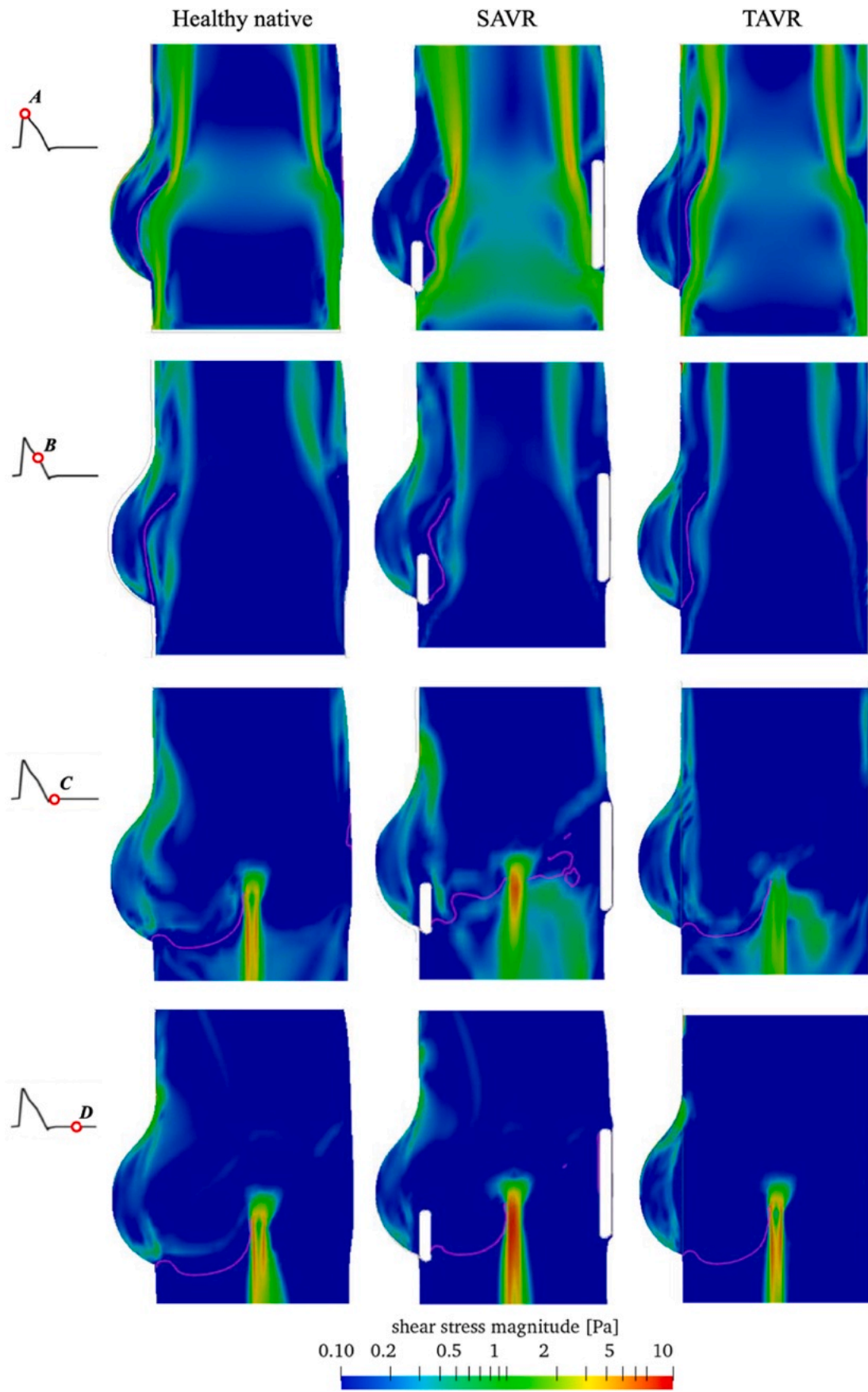
Fig. 10. Fluid shear stress magnitude contour maps for healthy native, SAVR and TAVR models.
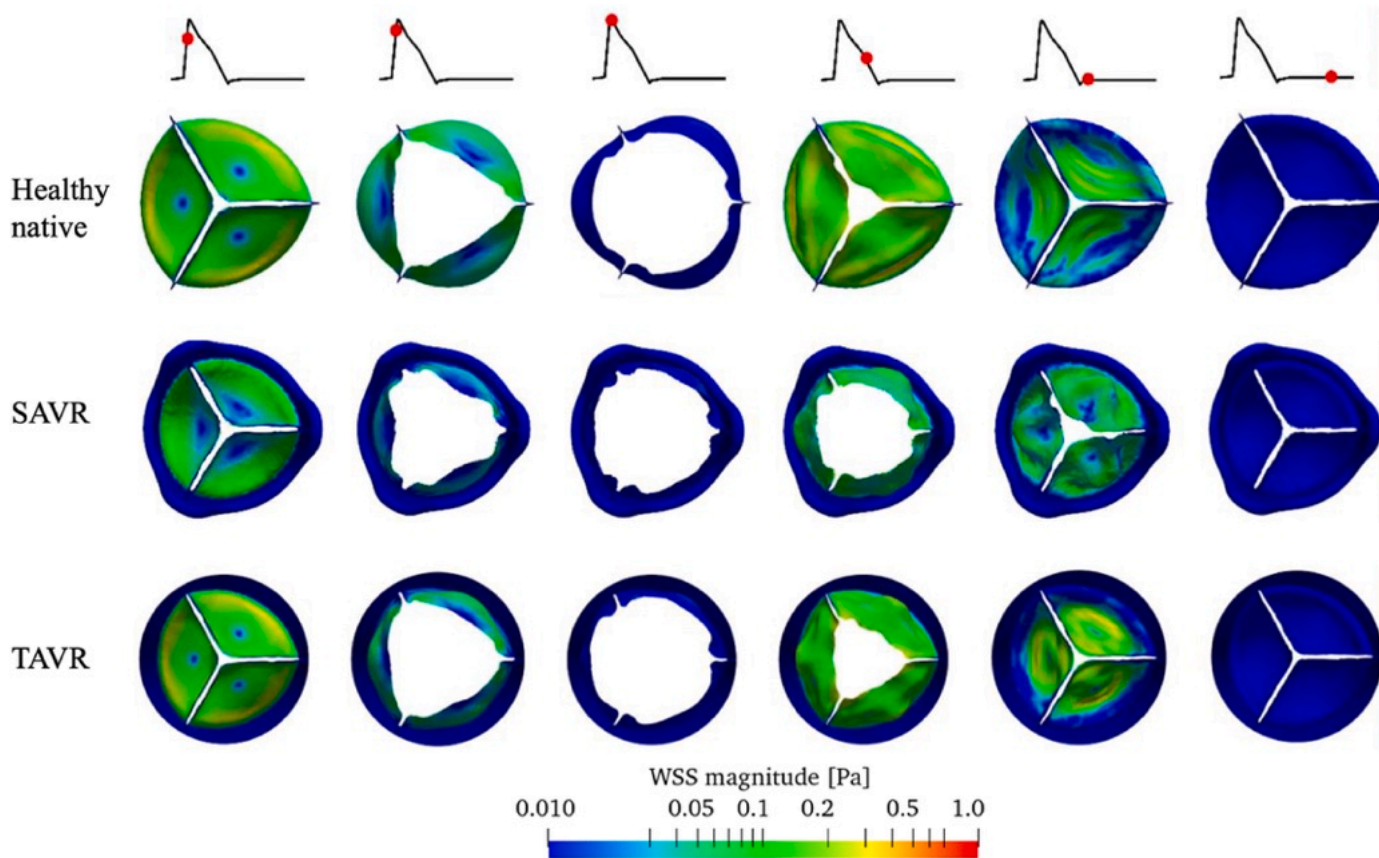
Fig. 11. WSS acting on the leaflets for healthy native, SAVR and TAVR models.

future efforts directed towards the development of improved valve designs aimed at restoring healthy conditions.

CRediT authorship contribution statement

Anna Maria Tango: Writing – original draft, Validation, Methodology, Investigation, Formal analysis, Data curation, Conceptualization. **Alessandra Monteleone:** Writing – original draft, Formal analysis, Data curation. **Andrea Ducci:** Writing – review & editing, Supervision, Resources, Methodology, Funding acquisition, Conceptualization. **Gaetano Burriesci:** Writing – review & editing, Supervision, Resources, Project administration, Methodology, Investigation, Funding acquisition, Formal analysis, Data curation, Conceptualization.

Declaration of competing interest

None Declared.

Acknowledgements

References

[1] V.T. Nkomo, J.M. Gardin, T.N. Skelton, J.S. Gottdiener, C.G. Scott, M. Enriquez-Sarano, Burden of valvular heart diseases: a population-based study, Lancet 368 (2006) 1005–1011, https://doi.org/10.1016/S0140-6736(06)69208-8.

[2] S. Coffey, R. Roberts-Thomson, A. Brown, J. Carapetis, M. Chen, M. Enriquez-Sarano, et al., Global epidemiology of valvular heart disease, Nat. Rev. Cardiol. 18 (2021) 853–864, https://doi.org/10.1038/s41569-021-00570-z.

[3] G.A. Roth, G.A. Mensah, C.O. Johnson, G. Addolorato, E. Ammirati, L.M. Baddour, et al., Global burden of cardiovascular diseases and risk factors, 1990–2019, J. Am. Coll. Cardiol. 76 (2020) 2982–3021, https://doi.org/10.1016/j.jacc.2020.11.010.

[4] C.W. Tsao, A.W. Aday, Z.I. Almarzooq, C.A.M. Anderson, P. Arora, C.L. Avery, et al., Heart disease and stroke statistics—2023 update: a report from the American heart association, Circulation 147 (2023), https://doi.org/10.1161/CIR.0000000000001123.

[5] F. Bakhtiary, O. Dzemali, U. Steinseiffer, C. Schmitz, B. Glasmacher, A. Moritz, et al., Opening and closing kinematics of fresh and calcified aortic valve prostheses: an in vitro study, J. Thorac. Cardiovasc. Surg. 134 (2007) 657–662, https://doi.org/10.1016/j.jtcvs.2007.02.050.

[6] H. Reul, A. Vahlbruch, M. Giersiepen, Th Schmitz-Rode, V. Hirtz, S. Effert, The geometry of the aortic root in health, at valve disease and after valve replacement, J. Biomech. 23 (1990) 181–191, https://doi.org/10.1016/0021-9290(90)90351-3.

[7] L.P. Dasi, H.A. Simon, P. Sucosky, A.P. Yoganathan, Fluid mechanics of artificial heart valves, Clin. Exp. Pharmacol. Physiol. 36 (2009) 225–237, https://doi.org/10.1111/j.1440-1681.2008.05099.x.

[8] G. Burriesci, F.C. Marincola, C. Zervides, Design of a novel polymeric heart valve, J. Med. Eng. Technol. 34 (2010) 7–22, https://doi.org/10.3109/03091900903261241.

[9] R. Toninato, J. Salmon, F.M. Susin, A. Ducci, G. Burriesci, Physiological vortices in the sinuses of Valsalva: an in vitro approach for bio-prosthetic valves, J. Biomech. 49 (2016), https://doi.org/10.1016/j.jbiomech.2016.05.027.

[10] A.P. Yoganathan, Z. He, S. Casey Jones, Fluid mechanics of heart valves, Annu. Rev. Biomed. Eng. 6 (2004) 331–362, https://doi.org/10.1146/annurev.bioeng.6.040803.140111.

[11] A. Zajarias, A.G. Cribier, Outcomes and safety of percutaneous aortic valve replacement, J. Am. Coll. Cardiol. 53 (2009) 1829–1836, https://doi.org/10.1016/j.jacc.2008.11.059.

[12] R. Guidoin, Y. Douville, M. Clavel, Z. Zhang, M. Nutley, P. Pîbarot, et al., The marvel of percutaneous cardiovascular devices in the elderly, Ann. N. Y. Acad. Sci. 1197 (2010) 188–199, https://doi.org/10.1111/j.1749-6632.2010.05517.x.

[13] J. Rodés-Cabau, Transcatheter aortic valve implantation: current and future approaches, Nat. Rev. Cardiol. 9 (2012) 15–29, https://doi.org/10.1038/nrcardio.2011.164.

[14] H. Ghanbari, A.G. Kidane, G. Burriesci, P. Bonhoeffer, A.M. Seifalian, Percutaneous heart valve replacement: an update, Trends Cardiovasc. Med. (2008), https://doi.org/10.1016/j.tcm.2008.02.002.

[15] P.S. Gunning, N. Saikrishnan, L.M. McNamara, A.P. Yoganathan, An in vitro evaluation of the impact of eccentric deployment on transcatheter aortic valve hemodynamics, Ann. Biomed. Eng. 42 (2014) 1195–1206, https://doi.org/10.1007/s10439-014-1008-6.

[16] J. Rodés-Cabau, E. Dumont, R.H. Boone, E. Larose, R. Bagur, R. Gurvitch, et al., Cerebral embolism following transcatheter aortic valve implantation, J. Am. Coll. Cardiol. 57 (2011) 18–28, https://doi.org/10.1016/j.jacc.2010.07.036.

[17] R.R. Makkar, G. Fontana, H. Jilaihawi, T. Chakravarty, K.F. Kofoed, O. De Backer, et al., Possible subclinical leaflet thrombosis in bioprosthetic aortic valves, N. Engl. J. Med. 373 (2015) 2015–2024, https://doi.org/10.1056/NEJMoa1509233.

[18] P. Kahlert, S.C. Knipp, M. Schlamann, M. Thielmann, F. Al-Rashid, M. Weber, et al., Silent and apparent cerebral ischemia after percutaneous transfemoral aortic valve implantation, Circulation 121 (2010) 870–878, https://doi.org/10.1161/CIRCULATIONAHA.109.855866.

[19] A. Ducci, S. Tzamtzis, M.J. Mullen, G. Burriesci, Hemodynamics in the Valsalva sinuses after transcatheter aortic valve implantation (TAVI), J. Heart Valve Dis. 22 (2013).

[20] A. Ducci, F. Pirisi, S. Tzamtzis, G. Burriesci, Transcatheter aortic valves produce unphysiological flows which may contribute to thromboembolic events: an in-vitro study 49 (2016) 4080–4089, https://doi.org/10.1016/j.biomech.2016.10.050.

[21] A.P. Yoganathan, K.B. Chandran, F. Sotiropoulos, Flow in prosthetic heart valves: state-of-the-art and future directions, Ann. Biomed. Eng. 33 (2005) 1689–1694, https://doi.org/10.1007/s10439-005-8759-z.

[22] K.B. Chandran, Role of computational simulations in heart valve dynamics and design of valvular prostheses, Cardiovasc Eng. Technol. 1 (2010) 18–38, https://doi.org/10.1007/s13239-010-0002-x.

[23] M.S. Sacks, A.P. Yoganathan, Heart valve function: a biomechanical perspective, Phil. Trans. Biol. Sci. 362 (2007) 1369–1391, https://doi.org/10.1098/rstb.2007.2122.

[24] O. Barannyk, P. Oshkai, The influence of the aortic root geometry on flow characteristics of a prosthetic heart valve, J. Biomech. Eng. 137 (2015), https://doi.org/10.1115/1.4029747.

[25] W. Mao, K. Li, W. Sun, Fluid–structure interaction study of transcatheter aortic valve dynamics using smoothed particle hydrodynamics, Cardiovasc Eng. Technol. 7 (2016) 374–388, https://doi.org/10.1007/s13239-016-0285-7.

[26] A. Laadhari, G. Székely, Eulerian finite element method for the numerical modeling of fluid dynamics of natural and pathological aortic valves, J. Comput. Appl. Math. 319 (2017) 236–261, https://doi.org/10.1016/j.cam.2016.11.042.

[27] A.M. Tango, J. Salmonsmith, A. Ducci, G. Burriesci, Validation and extension of a fluid–structure interaction model of the healthy aortic valve, Cardiovasc Eng. Technol. 9 (2018) 739–751, https://doi.org/10.1007/s13239-018-00391-1.

[28] A.M. Tango, A. Ducci, G. Burriesci, In silico study of the ageing effect upon aortic valves, J. Fluid Struct. 103 (2021) 103258, https://doi.org/10.1016/j.jfluidstructs.2021.103258.

[29] K.-M. Bornemann, S.E. Jahren, D. Obrist, The relation between aortic morphology and transcatheter aortic heart valve thrombosis: particle tracing and platelet activation in larger aortic roots with and without neo-sinus, Comput. Biol. Med. 179 (2024) 108828, https://doi.org/10.1016/j.compbiomed.2024.108828.

[30] V.B. Makhijani, H.Q. Yang, P.J. Dionne, M.J. Thubrikar, Three-dimensional coupled fluid-structure simulation of pericardial bioprosthetic aortic valve function, Am. Soc. Artif. Intern. Organs J. 43 (1997) M387–M392.

[31] J. De Hart, G.W.M. Peters, P.J.G. Schreurs, F.P.T. Baaijens, A three-dimensional computational analysis of fluid–structure interaction in the aortic valve, J. Biomech. 36 (2003) 103–112, https://doi.org/10.1016/S0021-9290(02)00244-0.

[32] J. De Hart, F.P.T. Baaijens, G.W.M. Peters, P.J.G. Schreurs, A computational fluid-structure interaction analysis of a fiber-reinforced stentless aortic valve, J. Biomech. 36 (2003) 699–712, https://doi.org/10.1016/S0021-9290(02)00448-7.

[33] C.J. Carmody, G. Burriesci, I.C. Howard, E.A. Patterson, An approach to the simulation of fluid–structure interaction in the aortic valve, J. Biomech. 39 (2006) 158–169, https://doi.org/10.1016/j.jbiomech.2004.10.038.

[34] G. Marom, R. Haj-Ali, E. Raanani, H.-J. Schäfers, M. Rosenfeld, A fluid–structure interaction model of the aortic valve with coaptation and compliant aortic root, Med. Biol. Eng. Comput. 50 (2012) 173–182, https://doi.org/10.1007/s11517-011-0849-5.

[35] F. Sturla, E. Votta, M. Stevanella, C.A. Conti, A. Redaelli, Impact of modeling fluid–structure interaction in the computational analysis of aortic root biomechanics, Med. Eng. Phys. 35 (2013) 1721–1730, https://doi.org/10.1016/j.medengphy.2013.07.015.

[36] G.B. Kalyana Sundaram, K.R. Balakrishnan, R.K. Kumar, Aortic valve dynamics using a fluid structure interaction model – the physiology of opening and closing, J. Biomech. 48 (2015) 1737–1744, https://doi.org/10.1016/j.jbiomech.2015.05.012.

[37] W. Wu, D. Pott, B. Mazza, T. Sironi, E. Dordoni, C. Chiastra, et al., Fluid–structure interaction model of a percutaneous aortic valve: comparison with an in vitro test and feasibility study in a patient-specific case, Ann. Biomed. Eng. 44 (2016) 590–603, https://doi.org/10.1007/s10439-015-1429-x.

[38] M.C.H. Wu, H.M. Muchowski, E.L. Johnson, M.R. Rajanna, M.-C. Hsu, Immersogeometric fluid–structure interaction modeling and simulation of transcatheter aortic valve replacement, Comput. Methods Appl. Mech. Eng. 357 (2019) 112556, https://doi.org/10.1016/j.cma.2019.07.025.

[39] X. Liu, W. Zhang, P. Ye, Q. Luo, Z. Chang, Fluid-structure interaction analysis on the influence of the aortic valve stent leaflet structure in hemodynamics, Front. Physiol. 13 (2022), https://doi.org/10.3389/fphys.2022.904453.

[40] A. Morany, K. Lavon, R. Gomez Bardon, B. Kovarovic, A. Hamdan, D. Bluestein, et al., Fluid–structure interaction modeling of compliant aortic valves using the lattice Boltzmann CFD and FEM methods, Biomech. Model. Mechanobiol. 22 (2023) 837–850, https://doi.org/10.1007/s10237-022-01684-0.

[41] S. Qashqaie Abdi, K. Hassani, The study of the relationship between unicuspid aortic valve insufficiency and heart disease by fluid-structure interaction modeling, Biomed. Eng. Adv. 5 (2023) 100079, https://doi.org/10.1016/j.bea.2023.100079.

[42] A. Monteleone, S. Di Leonardo, E. Napoli, G. Burriesci, A novel mono-physics particle-based approach for the simulation of cardiovascular fluid-structure interaction problems, Comput. Methods Progr. Biomed. 245 (2024) 108034, https://doi.org/10.1016/j.cmpb.2024.108034.

[43] W. Yan, J. Li, B. Zhang, W. Wang, L. Wei, H. Yu, et al., Patient-specific bicuspid aortic valve hemodynamics study based on computer simulation and in vitro experiment, Acta Mech. Sin. 40 (2024) 324022, https://doi.org/10.1007/s10409-024-24022-x.

[44] P. Corso, D. Obrist, On the role of aortic valve architecture for physiological hemodynamics and valve replacement, Part I: flow configuration and vortex dynamics, Comput. Biol. Med. 176 (2024) 108526, https://doi.org/10.1016/j.compbiomed.2024.108526.

[45] T. Qin, W. Mao, A. Caballero, N. Kamioka, S. Lerakis, S. Lain, et al., Patient-specific analysis of bicuspid aortic valve hemodynamics using a fully coupled fluid-structure interaction model, Comput. Biol. Med. 172 (2024) 108191, https://doi.org/10.1016/j.compbiomed.2024.108191.

[46] Y. Kim, W.K. Pyo, W.K. Kim, G.-Y. Suh, K. Kang, S.H. Lee, A parametric study regarding structural design of a bioprosthetic aortic valve by 3D fluid-structure interaction simulations, Heliyon 10 (2024) e27310, https://doi.org/10.1016/j.heliyon.2024.e27310.

[47] R. Xie, X. Han, T. Xiong, M. Chen, J.J.R. Williams, P. Lin, Numerical investigation of calcification effects on aortic valve motions and ambient flow characteristics, J. Fluid Struct. 124 (2024) 104014, https://doi.org/10.1016/j.jfluidstructs.2023.104014.

[48] A. Kheradvar, E.M. Groves, A. Falahatpisheh, M.K. Mofrad, S. Hamed Alavi, R. Tranquillo, et al., Emerging trends in heart valve engineering: Part IV. Computational modeling and experimental studies, Ann. Biomed. Eng. 43 (2015) 2314–2333, https://doi.org/10.1007/s10439-015-1394-4.

[49] J.O. Hallquist, LS-DYNA Theory Manual, Livermore Software Technology Corporation, 2006.

[50] M.M. Black, I.C. Howard, X. Huang, E.A. Patterson, A three-dimensional analysis of a bioprosthetic heart valve, J. Biomech. 24 (1991) 793–801, https://doi.org/10.1016/0021-9290(91)90304-6.

[51] I. Howard, E. Patterson, A. Yoxall, On the opening mechanism of the aortic valve: some observations from simulations, J. Med. Eng. Technol. 27 (2003) 259–266, https://doi.org/10.1080/0309190031000096621.

[52] Z.A. Wei, S.J. Sonntag, M. Toma, S. Singh-Gryzbon, W. Sun, Computational fluid dynamics assessment associated with transcatheter heart valve prostheses: a position paper of the ISO working group, Cardiovasc Eng. Technol. 9 (2018) 289–299, https://doi.org/10.1007/s13239-018-0349-y.

[53] LS-DYNA Aerospace Working Group, Modeling Guidelines Document, 2011.

[54] M. Thubrikar, The Aortic Valve, 1990. Boca Raton.

[55] A. Joda, Z. Jin, A. Haverich, J. Summers, S. Korossis, Multiphysics simulation of the effect of leaflet thickness inhomogeneity and material anisotropy on the stress–strain distribution on the aortic valve, J. Biomech. 49 (2016) 2502–2512, https://doi.org/10.1016/j.jbiomech.2016.02.041.

[56] S. Nobari, R. Mongrain, R. Leask, R. Cartier, The effect of aortic wall and aortic leaflet stiffening on coronary hemodynamic: a fluid–structure interaction study, Med. Biol. Eng. Comput. 51 (2013) 923–936, https://doi.org/10.1007/s11517-013-1066-1.

[57] E. Sirois, Q. Wang, W. Sun, Fluid simulation of a transcatheter aortic valve deployment into a patient-specific aortic root, Cardiovasc Eng. Technol. 2 (2011) 186–195, https://doi.org/10.1007/s13239-011-0037-7.

[58] R. De Paulis, A. Salica, Surgical anatomy of the aortic valve and root—implications for valve repair, Ann. Cardiothorac. Surg. 8 (2019) 313–321, https://doi.org/10.21037/acs.2019.04.16.

[59] I. Vesely, R. Noseworthy, Micromechanics of the fibrosa and the ventricularis in aortic valve leaflets, J. Biomech. 25 (1992) 101–113, https://doi.org/10.1016/0021-9290(92)90249-Z.

[60] T. Ishihara, V.J. Ferrans, M. Jones, S.W. Boyce, W.C. Roberts, Structure of bovine parietal pericardium and of unimplanted Ionescu-Shiley pericardial valvular bioprostheses, J. Thorac. Cardiovasc. Surg. 81 (1981) 747–757.

[61] A. Rassoli, N. Fatouraee, R. Guidoin, Z. Zhang, S. Ravaghi, A comparative study of different tissue materials for bioprosthetic aortic valves using experimental assays and finite element analysis, Comput. Methods Progr. Biomed. 220 (2022) 106813, https://doi.org/10.1016/j.cmpb.2022.106813.

[62] S. Bozkurt, G.L.G.L. Preston-Maher, R. Torii, G. Burriesci, Design, analysis and testing of a novel mitral valve for transcatheter implantation, Ann. Biomed. Eng. 45 (2017), https://doi.org/10.1007/s10439-017-1828-2.

[63] R. Gnyaneshwar, R.K. Kumar, K.R. Balakrishnan, Dynamic analysis of the aortic valve using a finite element model, Ann. Thorac. Surg. 73 (2002) 1122–1129, https://doi.org/10.1016/S0003-4975(01)03588-3.

[64] G.A. Holzapfel, T.C. Gasser, R.W. Ogden, A new constitutive framework for arterial wall mechanics and a comparative study of material models, J. Elasticity 61 (2000) 1–48, https://doi.org/10.1023/A:1010835316564.

[65] M.J. Thubrikar, Vascular Mechanics and Pathology, Springer US, Boston, MA, 2007, https://doi.org/10.1007/978-0-387-68234-1.

[66] European Committee for Standardization, Cardiovascular Implants—Cardiac Valve Prostheses (ISO 5840:2005), European Committee for Standardization, Washington, DC, 2005.

[67] A. Ranga, O. Bouchot, R. Mongrain, P. Ugolini, R. Cartier, Computational simulations of the aortic valve validated by imaging data: evaluation of valve-sparing techniques, Interact. Cardiovasc. Thorac. Surg. 5 (2006) 373–378, https://doi.org/10.1510/icvts.2005.121483.

[68] R.G. Leyh, C. Schmidtke, H.-H. Sievers, M.H. Yacoub, Opening and closing characteristics of the aortic valve after different types of valve-preserving surgery, Circulation 100 (1999) 2153–2160, https://doi.org/10.1161/01.CIR.100.21.2153.

[69] S. Nobari, R. Mongrain, E. Gaillard, R. Leask, R. Cartier, Therapeutic vascular compliance change may cause significant variation in coronary perfusion: a numerical study, Comput. Math. Methods Med. 2012 (2012) 1–10, https://doi.org/10.1155/2012/791686.

[70] B.J. Bellhouse, L. Talbot, The fluid mechanics of the aortic valve, J. Fluid Mech. 35 (1969) 721–735, https://doi.org/10.1017/S0022112069001406.

[71] A. Salica, G. Pisani, U. Morbiducci, R. Scaffa, D. Massai, A. Audenino, et al., The combined role of sinuses of Valsalva and flow pulsatility improves energy loss of the aortic valve, Eur. J. Cardio. Thorac. Surg. 49 (2016) 1222–1227, https://doi.org/10.1093/ejcts/ezv311.

[72] P.A. Midha, V. Raghav, I. Okafor, A.P. Yoganathan, The effect of valve-in-valve implantation height on sinus flow, Ann. Biomed. Eng. 45 (2017) 405–412, https://doi.org/10.1007/s10439-016-1642-2.

[73] P. Pibarot, J.G. Dumesnil, Doppler echocardiographic evaluation of prosthetic valve function, Heart 98 (2012) 69–78, https://doi.org/10.1136/heartjnl-2011-300351.

[74] J.D. Cleveland, M.E. Bowdish, C.E. Eberhardt, W.J. Mack, J.A. Crabtree, T. A. Vassiliades, et al., Evaluation of hemodynamic performance of aortic valve bioprostheses in a model of oversizing, Ann. Thorac. Surg. 103 (2017) 1866–1876, https://doi.org/10.1016/j.athoracsur.2016.10.019.

[75] W.R.E. Jamieson, L.H. Burr, R.T. Miyagishima, E. Germann, J.S. MacNab, E. Stanford, et al., Carpentier-Edwards supra-annular aortic porcine bioprosthesis: clinical performance over 20 years, J. Thorac. Cardiovasc. Surg. 130 (2005) 994–1000, https://doi.org/10.1016/j.jtcvs.2005.03.040.

[76] H. Maleki, S. Shahriari, M. Labrosse, J. Rodés-Cabau, P. Pibarot, L. Kadem, Effect of aortic annulus size and prosthesis oversizing on the hemodynamics and leaflet bending stress of transcatheter valves: an in vitro study, Can. J. Cardiol. 31 (2015) 1041–1046, https://doi.org/10.1016/j.cjca.2015.03.026.

[77] M. Külling, J. Külling, C. Wyss, D. Hürlimann, I. Reho, S. Salzberg, et al., Effective orifice area and hemodynamic performance of the transcatheter Edwards Sapien 3 prosthesis: short-term and 1-year follow-up, Eur Heart J. Cardiovasc Imag. 19 (2018) 23–30, https://doi.org/10.1093/ehjci/jew301.

[78] R.T. Hahn, P. Pibarot, W.J. Stewart, N.J. Weissman, D. Gopalakrishnan, M. G. Keane, et al., Comparison of transcatheter and surgical aortic valve replacement in severe aortic stenosis, J. Am. Coll. Cardiol. 61 (2013) 2514–2521, https://doi.org/10.1016/j.jacc.2013.02.087.

[79] L. Guimarães, P. Voisine, S. Mohammadi, D. Kalavrouziotis, E. Dumont, D. Doyle, et al., Valve hemodynamics following transcatheter or surgical aortic valve replacement in patients with small aortic annulus, Am. J. Cardiol. 125 (2020) 956–963, https://doi.org/10.1016/j.amjcard.2019.12.020.

[80] D. Angellotti, R. Manzo, D.S. Castiello, M. Immobile Molaro, A. Mariani, C. Iapicca, et al., Hemodynamic performance of transcatheter aortic valves: a comprehensive review, Diagnostics 13 (2023) 1731, https://doi.org/10.3390/diagnostics13101731.

[81] A.N. Azadani, N. Jaussaud, P.B. Matthews, L. Ge, T.S. Guy, T.A.M. Chuter, et al., Energy loss due to paravalvular leak with transcatheter aortic valve implantation, Ann. Thorac. Surg. 88 (2009) 1857–1863, https://doi.org/10.1016/j.athoracsur.2009.08.025.

[82] C.N. Bagot, R. Arya, Virchow and his triad: a question of attribution, Br. J. Haematol. 143 (2008) 180–190, https://doi.org/10.1111/j.1365-2141.2008.07323.x.

[83] G.D.O. Lowe, Virchow's triad revisited: abnormal flow, Pathophysiol. Haemostasis Thrombosis 33 (2003) 455–457, https://doi.org/10.1159/000083845.

[84] L.B. Leverett, J.D. Hellums, C.P. Alfrey, E.C. Lynch, Red blood cell damage by shear stress, Biophys. J. 12 (1972) 257–273, https://doi.org/10.1016/S0006-3495(72)86085-5.

[85] T. Chakravarty, L. Søndergaard, J. Friedman, O. De Backer, D. Berman, K. F. Kofoed, et al., Subclinical leaflet thrombosis in surgical and transcatheter bioprosthetic aortic valves: an observational study, Lancet 389 (2017) 2383–2392, https://doi.org/10.1016/S0140-6736(17)30757-2.

[86] E. De Marchena, J. Mesa, S. Pomenti, y Marin, C. Kall, X. Marincic, K. Yahagi, et al., Thrombus Formation following transcatheter aortic valve replacement, JACC Cardiovasc. Interv. 8 (2015) 728–739, https://doi.org/10.1016/j.jcin.2015.03.005.

[87] G. Pache, S. Schoechlin, P. Blanke, S. Dorfs, N. Jander, C.D. Arepalli, et al., Early hypo-attenuated leaflet thickening in balloon-expandable transcatheter aortic heart valves, Eur. Heart J. 37 (2016) 2263–2271, https://doi.org/10.1093/eurheartj/ehv526.

[88] N.C. Hansson, E.L. Grove, H.R. Andersen, J. Leipsic, O.N. Mathiassen, J.M. Jensen, et al., Transcatheter aortic valve thrombosis, J. Am. Coll. Cardiol. 68 (2016) 2059–2069, https://doi.org/10.1016/j.jacc.2016.08.010.

[89] R. Makkar, T. Chakravarty, Missing pieces of the transcatheter aortic valve replacement subclinical leaflet thrombosis puzzle, Circulation 146 (2022) 494–497, https://doi.org/10.1161/CIRCULATIONAHA.122.060422.

[90] F. D'Ascenzo, S. Salizzoni, A. Saglietto, M. Cortese, A. Latib, A. Franzone, et al., Incidence, predictors and cerebrovascular consequences of leaflet thrombosis after transcatheter aortic valve implantation: a systematic review and meta-analysis, Eur. J. Cardio. Thorac. Surg. (2019), https://doi.org/10.1093/ejcts/ezz099.

[91] O.K. Baskurt, M.R. Hardeman, M.W. Rampling, Handbook of Hemorheology and Hemodynamics, IOS press, 2007.

[92] Leonardo S. Di, D. Vella, C.S. Grillo, C. Martorana, S. Torre, V. Argano, et al., Hydrodynamic ex vivo analysis of valve-sparing techniques: assessment and comparison, Eur. J. Cardio. Thorac. Surg. 63 (2023), https://doi.org/10.1093/ejcts/ezad040.

[93] J.A. Salmonsmith, A. Ducci, G. Burriesci, Does transcatheter aortic valve alignment matter? Open Heart 6 (2019) e001132 https://doi.org/10.1136/openhrt-2019-001132.